JGR Oceans

RESEARCH ARTICLE
10.1029/2021JC017614

Forecasting the Gulf Stream Path Using Buoyancy and Wind Forcing Over the North Atlantic

Adrienne Silver[1], Avijit Gangopadhyay[1], Glen Gawarkiewicz[2], Arnold Taylor[3], and Alejandra Sanchez-Franks[4]

[1]School for Marine Science and Technology, University of Massachusetts Dartmouth, New Bedford, MA, USA, [2]Woods Hole Oceanographic Institution, Falmouth, MA, USA, [3]Plymouth Marine Laboratory, Plymouth, UK, [4]National Oceanography Centre, Southampton, UK

Key Points:

- The Parsons-Veronis hypothesis on the separation of the Gulf Stream appears to hold true for at least the last 40 years (1980–2019)
- The forecasting model of the Gulf Stream path (75–65W) uses the previous year's path, space-time integrated winds, and Icelandic low location
- The model shows a correlation of 0.65 for its 1-year forecast compared to the actual path for the years 1994–2020

Correspondence to:
A. Silver,
asilver@umassd.edu

Citation:
Silver, A., Gangopadhyay, A., Gawarkiewicz, G., Taylor, A., & Sanchez-Franks, A. (2021). Forecasting the Gulf Stream path using buoyancy and wind forcing over the North Atlantic. *Journal of Geophysical Research: Oceans*, *126*, e2021JC017614. https://doi.org/10.1029/2021JC017614

Received 29 MAY 2021
Accepted 26 JUL 2021

Abstract Fluctuations in the path of the Gulf Stream (GS) have been previously studied by primarily connecting to either the wind-driven subtropical gyre circulation or buoyancy forcing via the subpolar gyre. Here we present a statistical model for 1 year predictions of the GS path (represented by the GS northern wall—GSNW) between 75°W and 65°W incorporating both mechanisms in a combined framework. An existing model with multiple parameters including the previous year's GSNW index, center location, and amplitude of the Icelandic Low and the Southern Oscillation Index was augmented with basin-wide Ekman drift over the Azores High. The addition of the wind is supported by a validation of the simpler two-layer Parsons-Veronis model of GS separation over the last 40 years. A multivariate analysis was carried out to compare 1-year-in-advance forecast correlations from four different models. The optimal predictors of the best performing model include: (a) the GSNW index from the previous year, (b) gyre-scale integrated Ekman Drift over the past 2 years, and (c) longitude of the Icelandic Low center lagged by 3 years. The forecast correlation over the 27 years (1994–2020) is 0.65, an improvement from the previous multi-parameter model's forecast correlation of 0.52. The improvement is attributed to the addition of the wind-drift component. The sensitivity of forecasting the GS path after extreme atmospheric years is quantified. Results indicate the possibility of better understanding and enhanced predictability of the dominant wind-driven variability of the Atlantic Meridional Overturning Circulation and of fisheries management models that use the GS path as a metric.

Plain Language Summary The position of the Gulf Stream (GS), the western boundary current in the North Atlantic, after it detaches from the coast can affect processes from fisheries to atmospheric events and is an indicator of climate change. In this study, we were able to create a forecasting model predicting the position of the northern wall of the GS 1 year in advance. This model incorporated integrated winds generated from the Azores High and the Icelandic low, the two major atmospheric pressure centers over the North Atlantic. The correlation between the predicted latitude from the model with the observed GS North Wall index for over 27 years is 0.65. The ability to correctly predict the GS path has important implications for improving the management of Living Marine Resources.

1. Introduction

In the North Atlantic subtropical gyre, the Gulf Stream (GS) is the northward flowing geostrophic current that is topographically bound until it reaches the latitude of Cape Hatteras, where it separates from the coast and becomes a "free-wheeling" jet. The latitudinal excursion of the GS meanders from its mean path are on the order of 100–200 km after it departs from the coast (Cornillon, 1986). This path variability has been linked to multiple processes spanning from fisheries (Nye et al., 2011) to atmospheric events (Joyce et al., 2009) and is often interpreted as an indicator of climate change (Caesar et al., 2018; Zhang et al., 2019). In particular recent rapid changes in the northwest Atlantic water properties and ecosystem, responses have been linked to the variations of the GS path and its instabilities (Andres, 2016; Brickman et al., 2018; Gangopadhyay et al., 2019; Gawarkiewicz et al., 2012, 2018, 2019; Mills et al., 2013; Pershing et al., 2015; Silver et al., 2021).

The path of the GS from the separation point up to 65°W and beyond has often been quantified with one single metric—called the GS North Wall (GSNW) Index. The GSNW at the surface is defined by the sharp

temperature gradient that occurs where warm waters at the northern edge of the GS meet the cooler waters from the Slope Sea. A recent review of different metrics and their inter-relationship with respect to the GS axis is given by Chi et al. (2019).

The meandering of the GS path is also linked with its separation near Cape Hatteras (75°W, 35°N). The separation of the GS from the coast at Hatteras is governed by multiple factors such as inertial control (Fofonoff, 1954), basin-wide wind stress (Dengg, 1996; Gangopadhyay et al., 1992; Gill, 1982; Parsons, 1969; Veronis, 1973) and bathymetric control (Schoonover et al., 2017; Zhang & Vallis, 2007). The Taylor-Stephens Index (TSI ; see Data for details), an index of the GSNW (Taylor et al., 1998) has been shown previously to correlate well with the separation point inter-annually (Taylor & Gangopadhyay, 2001).

Previous studies have focused on two distinctly separate but somewhat linked force-response mechanisms between the GS path and the overlying wind system. First, the Parsons-Veronis hypothesis is built on the concept of separation by detachment. This theory, within a two-layer ocean model, implies that the GS detaches from the coast when it reaches a latitude in which the boundary between the two layers extends to the surface, essentially at an outcropping of isopycnals (Huang & Flierl, 1987; Parsons, 1969; Veronis, 1973). This hypothesis was tested by Gangopadhyay et al. (1992) (GCW92, hereafter), who found evidence that the observed separation latitude of the GS was correlated with the predicted outcropping latitude (OCL) of the two-layer model if one integrates the wind-stress over the subtropical Atlantic basin (dominated by Azores High) for 3 years. This 3-year time-period was attributed to the integrating effect of long-planetary Baroclinic Rossby Waves (BRW) to cross the Atlantic and affect the western boundary (Gill, 1982).

Furthermore, the path of the GS after separation is dependent on the separation point itself. It is well known that the GS has a standing meander pattern between 75°W and 70°W (Cornillon, 1986; Lee & Cornillon, 1996; Tracey & Watts, 1986). Thus the latitude and angle of the GS at separation dictates the path of the GS at least up to 70°W; indicting that the choice of TSI as a metric of separation as well as a GSNW index (at least for the western half of the GS between 75 and 65°W) is reasonable.

A number of studies have proposed that the path of the GS is influenced by the southward flow of Labrador Seawater (Rossby, 1999), dictated by the strength and location of one of the North Atlantic Oscillation (NAO)'s Center of Action, the Icelandic low-pressure center (Hameed & Piontkovski, 2004; Sanchez-Franks et al., 2016). Sanchez-Franks et al. (2016) (SHW16 hereafter) created a regression prediction method of forecasting the GSNW position 1-year ahead using Icelandic low center pressure and longitude paired with the Southern Oscillation Index (SOI). SHW16 found that the forecasted GSNW values accounted for 36% of the variance and did not consider other mechanisms, for example, the latitude of separation, that could influence the GS location.

The variability of the path and transport (of heat and mass) of the GS is also linked to the variability of the Atlantic Meridional Overturning Circulation (AMOC). Understanding the GS path variability, a component of the AMOC, might lead to a better understanding and prediction of the variability of the overall AMOC (Caesar et al., 2021; Lozier, 2010). A number of studies have recently suggested that the impacts of buoyancy and wind forcing on the AMOC transport are different over different time-scales; wind-forcing dominating the seasonal, interannual and decadal variability while the buoyancy forcing dominates over the longer, centennial time-scales (Biastoch et al., 2008; Mielke et al., 2013; Zhao & Johns, 2014a, 2014b). Using data (2004–2010) and model simulations, both Zhao and Johns (2014a, 2014b) and (Mielke et al., 2013) concluded that although it is a relatively smaller constituent of the total AMOC transport, most of the AMOC variability results from the Ekman transport component.

Mooring array programs at both 26°N (Smeed et al., 2016, RAPID) and 53°N (Lozier et al., 2017, OSNAP) show that the variability of the Ekman transport is about $\pm 1.5 - 2$ Sv, while the amplitude and seasonal range is about $3 - 4$ Sv. Thus, it makes a case for understanding the variability of the Ekman transport which is restricted to the upper layer of the AMOC. In turn, in a simple 2-layer Parsons-Veronis model sense, this Ekman drift is related to the separation and path of the GS at the western boundary between 26° N and 41°N.

In summary, the wind-driven GS, resulting from integrated effects of basin-scale wind gyres (Gangopadhyay et al., 1992, 2016) flowing around the two atmospheric Centers of Action (i.e., the Icelandic Low and the

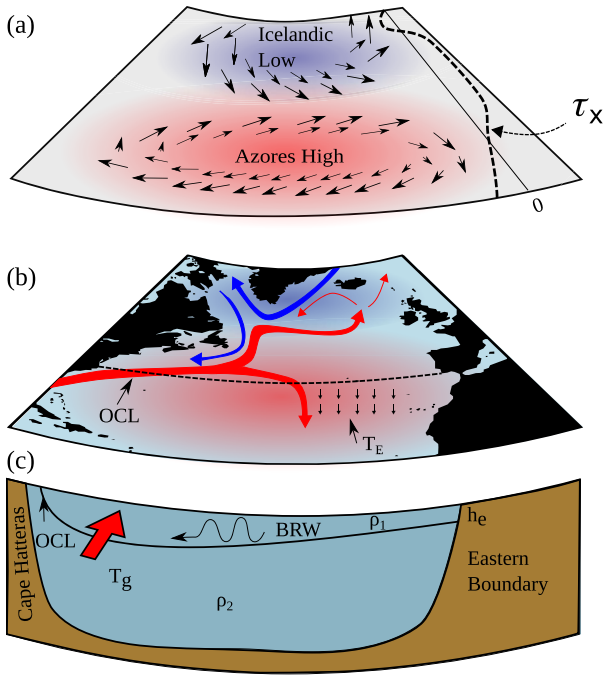

Figure 1. This synergistic schematic shows the different aspects of atmospheric forcing and their influence on the Gulf Stream (GS) which are incorporated into the forecasting model. (a) The two components of the North Atlantic Oscillation (AH and IL) are presented with wind vector arrows while the dashed line on the right edge shows the typical latitudinal variation of the zonal wind stress, τ_x. (b) The surface circulation with the red arrows represents the GS and the North Atlantic Current; the blue arrows represent the Labrador current and other currents around Greenland. The small black arrows show the southward Ekman drift (T_E) under the Azores High. The dashed line shows the location of the outcropping latitude (OCL) along which the vertical depth structure is depicted in the bottom panel. (c) The depth structure of the two-layer ocean model with the OCL marked on the western side is shown here. The geostrophic flow is marked by the red arrow and the interface between the two boundaries on the eastern side is marked by h_e. BRW represents the Baroclinic Rossby Waves. The image was generated using Inkscape (Inkscape Project, 2020) and MATLAB's mapping toolbox (The MathWorks, 2020).

Azores High) of the NAO, is sensitive to both atmospheric pressure cells. A schematic in Figure 1 captures this synergistic force-response system of the GS path to both the components of the NAO via their respective forcing parameters. The GS is situated at the boundary between the subtropical and subpolar gyres. The variability of the GS path is thus partly due to (a) the basin-scale wind-driven through long BRW and the latitude of separation as per GCW92 associated with the Azores High and (b) the buoyancy advection of Labrador Current and Labrador Sea Water from the Labrador Sea region (Joyce et al., 2009), associated with the Icelandic Low as per SHW16.

We present a statistical model for the first time whose parameters represent the effects of buoyancy and wind-forcing in a combined response system for predicting the variability of the GS path using 40 (1980–2019) years of observed wind and 41 years (1980–2020) of GS index data. Specifically, we will be first exploring the hypothesis proposed by Parsons (1969) and Veronis (1973) and building upon the work done by Gangopadhyay et al. (1992), reanalyzing the hypothesis over a longer time (40 years). We then combine the Parsons-Veronis hypothesis (wind-forcing) with influences of the Icelandic Low (bringing in the buoyancy-forcing by extending the previous work by SHW16) to develop a new forecasting model for the path of the GS.

The organization of this paper is as follows. Section 2 outlines the different data sets used in this study. Section 3 presents the validation of the Parsons-Veronis mechanism of predicting the outcropping latitude for the 40-year period (1980–2019). A hierarchical forecast model development is presented in Section 4 starting from the SHW16 model and ending with a model that incorporates both the effects of integrated wind stress over subtropical Atlantic and the longitudinal movement of the Icelandic Low. Additional parameters such as the SOI and the Icelandic Low Pressure (ILP) amplitude are included in intermediate steps to test the sensitivity of the GS response to extreme conditions of the El Niño Southern Oscillation and NAO variability. Section 4 also discusses these sensitivities and Section 5 summarizes the results with implications to the presently active AMOC.

2. Data

In this section, we briefly describe the different data sets used in this study: (a) the GS path and (b) multiple parameters from the atmospheric system.

2.1. GS Path

The Taylor-Stephens index (TSI) was calculated by applying principal components analysis to the time series of monthly latitudes of the north wall at (79, 75, 72, 70, 67, and 65°W), and found to be significantly linked to the NAO (Taylor & Gangopadhyay, 2001; Taylor et al., 1998).

The TSI in addition to being used as a measurement of the GSNW is also used here as an estimation of the GS separation latitude. We validated this by comparing the TSI with the Atlantic Zone Mapping Program's (AZMP) (Fisheries and Oceans Canada, 2021) GS location at 74°W and with the location of the 50 cm contour line from AVISO sea surface height fields at 74°W (Global Monitoring and Forecasting Center, 2021). Both comparisons, AZMP and AVISO, showed high correlations with the TSI ($r = 0.74$ and 0.66, respectively, for the period 1993 to 2016) as seen in Figure 2 justifying our usage of TSI as a proxy for the separation latitude.

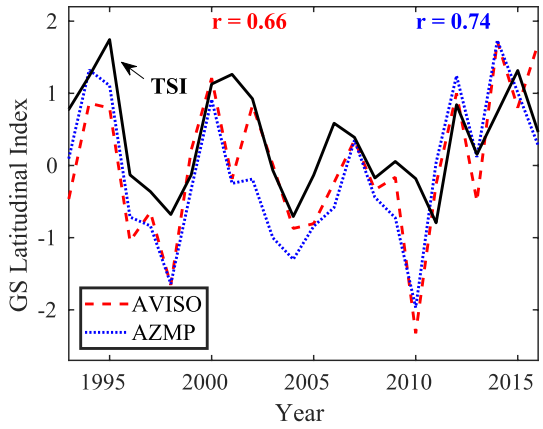

Figure 2. Validating the Taylor-Stephen Index (TSI) with two different metrics of the Gulf Stream separation latitude at 74°W. The Atlantic Zone Mapping Program (AZMP) uses sea surface temperature and the AVISO quantification uses the 50 cm contour from sea surface height fields. The correlations between the AVISO separation and with the TSI and the AZMP with the TSI are $r = 0.66$ (red text in figure) and $r = 0.74$ (blue text in figure), respectively, for the period 1993 to 2016.

2.2. Atmospheric Forcing Related Data

The wind stress data was obtained from JRA-55 yearly wind fields which are available from 1958 to 2019 at a 1.25° grid (Japan Meteorological Agency, 2013). This is higher resolution than the 2.5° wind used in GCW92. The JRA-55 wind data are available from https://rda.ucar.edu/datasets/ds628.1/. The SOI data are available from https://climatedataguide.ucar.edu/climate-data/southern-oscillation-indices-signal-noise-and-tahitidarwin-slp-soi (Trenberth, 1984). The atmospheric centers of action indices (for Azores High and Icelandic Low) are available from https://you.stonybrook.edu/coaindices/ (Hameed & Piontkovski, 2004; Hameed & Riemer, 2012). The NAO winter index is available from https://climatedataguide.ucar.edu/climate-data/hurrell-north-atlantic-oscillation-nao-index-station-based (Hurrell et al., 2003).

Finally, the analysis time-period for the Parsons-Veronis model focusing on validating the linkage between the GS path and the Azores High winds (in an integrated sense) was the 40-year period (1980–2019). The forecasting model was fit over the 14-year period 1980–1993, and the 1-year forecast comparisons were carried out over the next 27-year period (1994–2020). Extreme years for SOI, ILL, and NAO were identified as those years when the parameters were beyond ±0.8 standard deviation from their mean value over the 1980–2019 period.

3. The Variability of the GS Separation Latitude (1980–2019)

3.1. The Parsons-Veronis Model (Wind-Forcing)

Following GCW92's methodology, we considered a two-layer ocean forced by steady wind stress with the bottom layer at rest. Using a balance between Ekman transport and the northward geostrophic flow, the outcropping latitude was predicted. The model was constructed using the equations from GCW92 with the final form being:

$$\frac{g'}{2f}h_w^2 = \frac{g'}{2f}h_e^2 - T_E \tag{1}$$

The term $\frac{g'}{2f}h_e^2$ represents the geostrophic transport and $g' = \frac{g(\rho_2 - \rho_1)}{\rho_2}$ is the reduced gravity of the two-layer model with ρ_1 and ρ_2 being the densities of the upper and lower layers and f being the Coriolis parameter. Depths of the interface between the two layers at the eastern and western boundaries are represented by h_e and h_w, respectively. The outcropping latitude is obtained by setting $h_w = 0$, so that the isopycnal reaches the surface at the western boundary. This eliminates the left hand side of Equation 1 and establishes a balance between the northward geostrophic flow and the Ekman transport. Ekman transport increases as one moves further North, so in order to maintain this balance the GS has to detach from the coast and move eastward. In this way, we can use this equation to predict the separation latitude (as the outcropping latitude) of the GS. The h_e and ρ values were based on the GCW92 work which designed a data-based two-layer system of the subtropical north Atlantic using CTD casts (conductivity, temperature, and depth) from the National Oceanographic Data Center database. Specifically, $\rho_1 = 1026.4\, kgm^{-3}$ and $\rho_2 = 1027.61\, kgm^{-3}$, which yielded a $g' = 0.0115\, ms^{-2}$. The values of h_e were adapted from the CTD-based two-layer model presented by GCW92 and are interpolated to higher resolution grid for this study. The original values of h_e were 375, 300, 230, and 125 m at 31°N, 33°N, 37°N, and 41°N respectively.

The Ekman Transport was computed by integrating the zonal wind stress (τ_x) from 20°W to 75°W, excluding regions over land. GCW92 used a constant 110 km per degree longitude and a constant f value, equivalent to f at 35°N, for all latitudes. This was updated here by allowing for both longitudinal distance variations

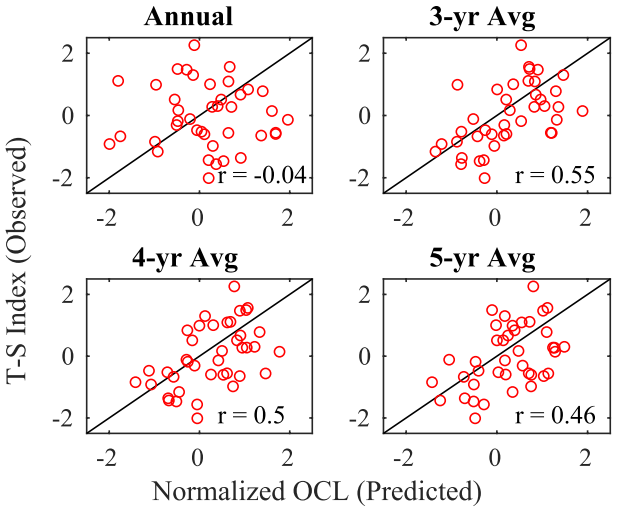

Figure 3. Correlation (r) between predicted separation latitudes using JRA-55 winds averaged annually, and with 3, 4, and 5 years running averages against the observed Gulf Stream Northern Wall (Taylor-Stephens Index). The 3-, 4-, and 5-year averaged correlations are significant. OCL, outcropping latitude.

over spherical earth and for f to vary with latitude. The Ekman transport T_E in Sv was then calculated using the equation

$$T_E = \frac{\int_{x_E}^{x_W} \tau_x dx}{\rho_1 f} \quad (2)$$

where ρ_1 is the density of the surface layer (1,026.4 kgm^{-3}) and τ_x is integrated from 75°W (x_W) to 20°W (x_E).

Note that, Zhao and Johns (2014a, 2014b) set up a simple two layer model to understand the seasonal and interannual variability of the AMOC and found credence to the dominance of wind-driving in explaining its observed variability in both time-scales. The present data-based model set up for validating the Parsons-Veronis hypothesis is very similar to that of Zhao and Johns (2014a, 2104b) two-layer numerical model set with wind forcing. It is thus reasonable to test and validate the variability of the path of the GS based on a simpler Parsons-Veronis hypothesis with a two-layer model in the presence of a robust and active AMOC.

Wind stress acting on a thermocline generates planetary waves that propagate to the west (Anderson & Corry, 1985). Given that the time scale for planetary waves moving across the North Atlantic (with speeds of ≈ 3.7 km day^{-1}) is on the order of 3–5 years (Gill, 1982; Halliwell & Cornillon, 1990), it is not expected that a significant correlation between prediction and observation will be obtained when the annual wind is used to predict the outcropping latitude. A correlation was expected once this time integration scale is accounted for as was the case in GCW92. For this reason, running averages of 3, 4, and 5 years were conducted on T_E values which were then used to calculate the predicted outcropping latitude. For example, for a 3-year running average, an average of T_E values from 1991, 1992, and 1993 would be used to predict the outcropping latitude for 1993 and be compared to the observed north wall position (TSI) in 1993.

All reported p-values were calculated with an adjusted sample size to account for autocorrelation. This was done using the equation from Quenouille (1951) given below and following the methodology of Taylor (1995) and SHW16:

$$N' = N \,/\, (1 + 2r_1 r_1' + 2r_2 r_2' + \ldots) \quad (3)$$

where N is the unadjusted number of points in each time series and r_1 and r_1' are the lag one autocorrelations of the respective time series, and r_2 and r_2' are the 2-year lag autocorrelations. While investigating the outcropping latitude, this calculation included terms up to r_4, because the addition of higher-order autocorrelations had a negligible effect on the p-values.

3.2. Predicted Outcropping Latitude Versus Observed GSNW Index

The outcropping latitudes predicted on the basis of the Parsons-Veronis hypothesis are correlated with the GSNW position given by the TSI over the years 1980–2019 when averaged over a 3-year period. Figure 3 shows the comparisons between the predicted outcropping latitude and the TSI for the years 1980–2019 with annual and 3, 4, and 5-year running averages. Similar to GCW92 results, the annual averages showed an insignificant correlation between the predicted outcropping latitude and observed separation locations (TSI) ($r = -0.04$, $p = 0.84$). When a 3-year running average was applied to T_E, a strong correlation emerges for the year-to-year comparison between TSI and Parsons-Veronis prediction, with $r = 0.55$ $p = 0.012$. The 4- and 5-year running averages also show similar correlations with the observed TSI; however, the correlation coefficients slightly decrease, and the p-values increase with an increased averaging period after 3 years, matching what was observed in GCW92. The 3-year integrated wind-based predictions of the outcropping separation latitude from Equation 1 also showed significant correlations with the AZMP and AVISO with $r = 0.44$ ($p = 0.023$) and $r = 0.44$ $p = 0.105$), respectively.

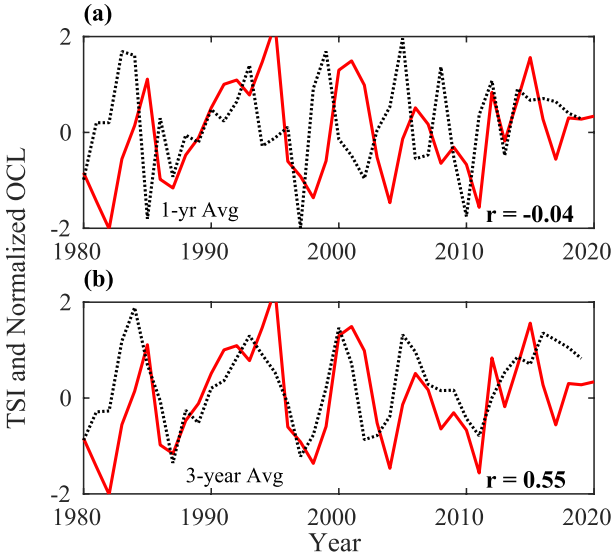

Figure 4. Comparison of Taylor-Stephens Index (red solid line) with normalized predicted outcropping latitudes (black dashed line) based on (a) annual averaged winds and (b) 3-year running average winds from 1980 to 2019.

This increased correlation with 3-year averaging is also shown in Figures 4a and 4b. Figure 4a shows the annual average with an apparent lag between the outcropping latitude and the observed one. Figure 4b then shows the outcropping latitudes with 3-year averaging, closing this gap between outcropping and observed latitudes due to the delayed integrated effect of the generated planetary waves.

It is worth pointing out the connection between the "lost fluid" in the upper layer of the original 2-layer Parsons-Veronis equations (see Equation 9 of GCW92) and the uncertainties in AMOC transports. The AMOC has a mean flow around 18 Sv at 26°N and around 13 Sv at 41°N, in comparison the Ekman transport variations of around 2–4 Sv might seem insignificant (Mielke et al., 2013). As mentioned before, the majority of the interannual variability is driven by fluctuations in wind stress (Frajka-Williams et al., 2019; Zhao & Johns, 2014b).

Using the latitudinal difference between the known separation latitude from AZMP and our predictions, a yearly estimate of the loss of fluid in the two layer model was obtained with a mean of 0.8 Sv and a range of 0.04 – 1.6Sv. These numbers match well with the 0.7–4.9 Sv found to be lost in the observed range of AMOC-Ekman transport between 26°N and 41°N (Mielke et al., 2013).

4. A Forecast Model for the Path of the GS

4.1. Icelandic Low Model (Buoyancy Forcing)

The strength of the NAO directly influences the North Atlantic circulation (Hurrell et al., 2000, 2001; Walker & Bliss, 1932). Many recent studies (Drinkwater, 2004; Drinkwater et al., 2003; Hameed & Piontkovski, 2004; Rossby, 1999; Rossby & Benway, 2000, SHW16) have focused their attention on the lag time scale between the advection from the Labrador Sea and the latitudinal variation of the GS path. Mechanisms such as forcing by the Deep Western Boundary Current (Spall, 1996; Thompson & Jr, 1989) connected with the Labrador convection region and the movement of the Icelandic low (Hameed & Piontkovski, 2004) have been suggested.

SHW16 developed a regression-based forecasting model incorporating the hypothesis of the Icelandic low forcing the Labrador Sea water into the Slope Sea from Hameed and Piontkovski (2004) and the influence of the SOI from Taylor et al. (1998). For a 1-year forecasting model, SHW16 obtained the best regression equation for the "i"th year prediction as follows,

$$GSNW_i = a\,GSNW_{i-1} + b\,ILP_{i-2} + c\,ILL_{i-3} + d\,SOI_{i-2} + e \qquad \text{Model A} \tag{4}$$

where $GSNW$ is the GS north wall position from the TSI, ILP and ILL are the average Icelandic Low pressure and longitude from December through February respectively, and SOI is the average SOI from September through February for the subscript year. The multipliers a, b, c, and d are the regression coefficients, while e is the residual. We were able to reproduce the results from SHW16 as well as extend the model prediction through 2020 (Tables 1 and 2 and Figure 5; for data sources, see Section 2).

4.2. Combined Icelandic Low-Azores High Model (Buoyancy and Wind Forcing)

Motivated by the validation of the Parsons-Veronis mechanism for over the last 40 years as shown in Section 3, a new model that incorporates both the Icelandic Low and the basin-wide, time-integrated wind-driven predicted outcropping latitude information is proposed. This is the novelty of this work. It connects the two pressure cells of the Atlantic wind system: (a) Icelandic Low Center longitude's east-west excursion with a lag of multiple years and (b) Azores High component contributing through the basin-wide time-integrated Ekman wind drift as modeled by the Parsons-Veronis hypothesis. A series of experiments were carried out with different combinations of the longitudinal variation of the Icelandic Low, basin-wide wind

Table 1
Standardized Beta Coefficients of Model Variables for Models A, B, C, and D Fit From 1980 to 2020

Model	$GSNW_{i-1}$	$OCL2_{i-1}$	ILP_{i-2}	ILL_{i-3}	SOI_{i-2}	r_f	p-value
A	0.42*	NA	−0.10	−0.24*	0.04	0.52	0.029
B	0.33*	0.31*	−0.04	−0.17*	0.04	0.65	0.007
C	NA	0.36*	−0.12	−0.11	0.04	0.61	0.007
D	0.33*	0.32*	NA	−0.16*	NA	0.65	0.016

Note. Coefficient values with an asterisk indicate significance at a 95% level. The r_f is the correlation coefficient between 1-year model predictions and the TSI; the corresponding p-value is listed in the last column.
Abbreviation: TSI, Taylor-Stephen Index.

stress integrated over 2–3 years and the SOI. We present the results in Tables 1 and 2 and discuss them below.

While the 3-year integration timescale works well for validating the Parsons-Veronis mechanism, a forecast model for year "i" does not have the wind information for the forecast year. Given the need for 1 year in advance prediction without knowing next year's winds, predicted outcropping latitudes based on 2 years of wind-integration were used with a 1-year lag. The addition of the 2-year integrated wind-derived outcropping latitude ($OCL2$) into Model A created a new model, Model B which can be given as follows

$$GSNW_i = a\,GSNW_{i-1} + b\,OCL2_{i-1} + c\,ILP_{i-2} + d\,ILL_{i-3} + e\,SOI_{i-2} + f \quad \text{Model B} \tag{5}$$

Following the methodology from SHW16, the model fit was assessed by making continual 1-year predictions for 1994 through 2020 and then comparing the correlation and mean absolute error (MAE) between forecast locations and the observed GSNW positions. Following SHW16, $MAE = \frac{1}{n}\sum_{i=1}^{n} | f_i - y_i |$ where f_i is the model's prediction and y_i is the observed GSNW position (TSI for the ith year). Both f_i and y_i time-series were standardized to compute the MAE. For each 1-year prediction, the model was fit from 1980 through 1 year prior to the prediction year. For example, the years 1980–1993 were used to fit the model and forecast for 1994. Similarly, the years from 1980 to 1994 were used to fit the model and forecast for 1995. This process was continued for all 1-year predictions from 1994 to 2020. The model is evaluated by calculating the correlation between its predictions with observations. To avoid confusion with other r values used in this paper, this correlation coefficient between model predictions and observations will be called the "forecast correlation" r_f from here on. Years 1980–1993 were not predicted as the model would not have enough data to robustly fit all variables (see SHW16) for 1-year advance prediction for those years. Table 1 presents the resulting r_f values and their corresponding p-values. The sample size

Table 2
Model Fit Parameters With r_f Being the Correlation Between the 1-Year Predictions and Observed TSI From 1994 to 2020, MAE Being the Mean Absolute Error of 1-Year Predictions, RV Being the Residual Variance Between Predictions and TSI, AICc Being the Akaike Information Criterion Adjusted for Small Sample Sizes for Each Model Fit to the Whole Time Series

Model	r_f	MAE	RV	AICc
A	0.52	0.64	0.70	68.3
B	0.65	0.54	0.53	59.3
C	0.61	0.53	0.54	63.1
D	0.65	0.50	0.40	57.0

Abbreviation: TSI, Taylor-Stephen Index.

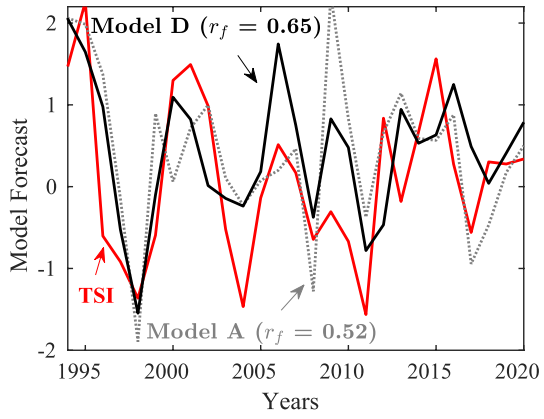

Figure 5. One-year model forecasts from Model A and D compared to Taylor-Stephens Index (TSI). The r_f values in the figures represent correlations between the TSI and the 1-year predictions from both forecast models. Note that the time-axis spans the forecast period (1994–2020).

was adjusted with autocorrelations up to 4 years in Equation 3 with the addition of further lagged autocorrelations having a negligible effect on the *p*-values.

The 1-year model prediction for Model B using the integrated outcropping latitude shows a strong correlation with TSI with an $r_f = 0.65$ and MAE = 0.54 over the forecast period (1994–2020). In comparison Model A has a $r_f = 0.52$ and MAE = 0.64. The correlation is increased and the MAE is decreased with the addition of the wind-integrated prediction of outcropping latitude.

To compare the relative contribution of each predictor variable to the outcome variable (*GSNW*) in the forecasting model, standardized beta coefficients are used. Beta coefficients show the degree of change in the outcome variable given one unit change of the predictor variable. So, beta coefficients with larger absolute values indicate larger influences on the outcome variable. Given that all our variables are normalized before going in to the model these are standardized beta coefficients with units of standard deviations. The final model can thus be selected using the beta coefficients from the different individual model experiments.

Both the $GSNW_{i-1}$ and $OCL2_{i-1}$ explain roughly the same amount of variance in Model B with beta coefficients of 0.33 and 0.31 respectively (Table 1). When the $GSNW_{i-1}$ variable was removed from Model B, creating Model C, the r_f value dropped to 0.61.

$$GSNW_i = a\,OCL2_{i-1} + bILP_{i-2} + cILL_{i-3} + dSOI_{i-2} + e \quad \text{Model C} \tag{6}$$

When both $GSNW_{i-1}$ and $OCL2_{i-1}$ were removed from Model B, the correlation between 1-year predictions and observed locations dropped to $r_f = 0.42$, showing the large contribution of the wind-integrated outcropping latitude in the model.

The Icelandic low pressure and *SOI* explain relatively less variance compared to other variables and are not significant in Model A or B. For this reason we built a new model with only the significant contributors, which is,

$$GSNW_i = a\,GSNW_{i-1} + b\,OCL2_{i-1} + c\,ILL_{i-3} + d \quad \text{Model D} \tag{7}$$

This model resulted in an r_f value of 0.65 for the whole forecast period of 1994–2020 (Figure 5). The reason that ILP and SOI were found to be significant in the SHW16 paper but not in any of the models in our study, is because of the difference in the time periods used to fit the model. SHW16 used data beginning in 1966 whereas we use data beginning in 1980 to fit the models. We restricted our analysis to the 40-year period after 1980 for two reasons. First, it is well known that there was relatively poor spatial coverage of the atmospheric data in the years before satellite observations started in 1979. This led to the poorer quality of wind products (due to coarser resolution of available data and spatial-temporal gaps), which have been well recognized by many studies recently (Huesmann & Hitchman, 2003; Kistler et al., 2001; Sturaro, 2003). Second, prior to the 1970s, the data used to calculate the GS indices were much more scarce, leading to potentially less accurate estimates of the GS north wall location (McCarthy et al., 2018). Furthermore, while testing the models for the period used in the SHW16 paper we found that even though the ILP and SOI are significant in Models A-C; Model D still performed best with a $r_f = 0.66$, compared to a $r_f = 0.57$ for Model A. The fidelity of Model D is attributed to the inclusion of both buoyancies forcing (ILL) and wind driving (OCL) effects to forecast the GS path.

In addition to evaluating the forecast correlation, two other tests were carried out to assess model fit, residual variance, and AICc (see Table 2). The residual variance is the sum of squares of the difference between the observation and the model predicted value (Weisberg, 2005). Model D showed a drop in residual variance compared to Model A, both when comparing the 1-year predictions to the observed TSI (0.40 and

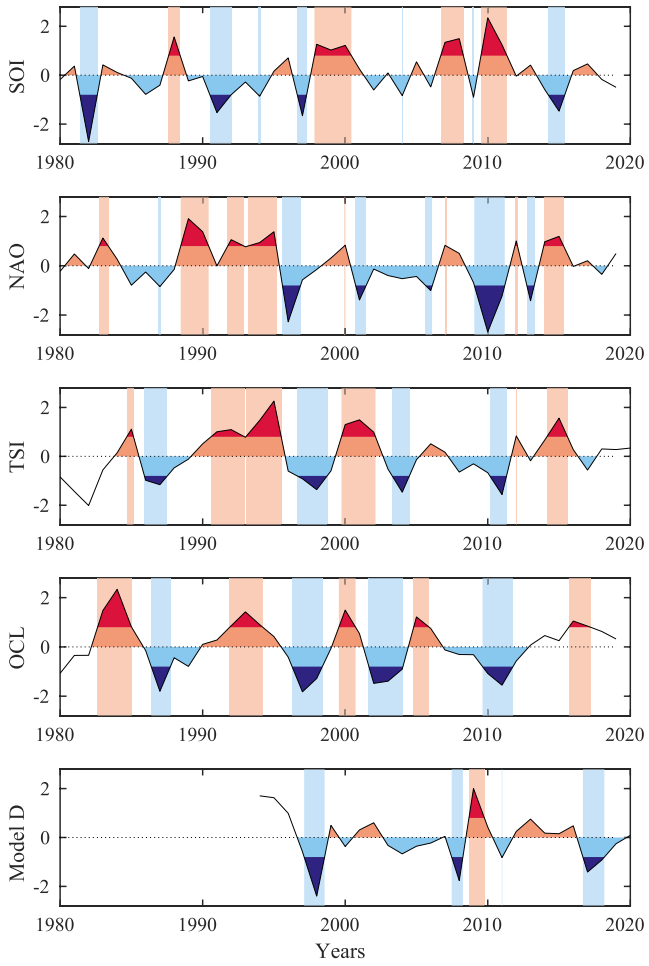

Figure 6. Time series of atmospheric indices Southern Oscillation Index (SOI), North Atlantic Oscillation (NAO), with extreme years (outside ±0.8 standard deviation) highlighted with vertical stripes and shown with shaded dark red or dark blue regions. All indices are normalized. The SOI is averaged over September through February and NAO is averaged over December through February. The TSI is the annual Taylor-Stephens Index, the outcropping latitude (OCL) is the 3-year integrated predicted outcropping latitude, and Model D is the 1-year forecast from the final model.

0.70, respectively) and when comparing the model when fit with all available years to the TSI (0.27 and 0.34, respectively).

Since there was a varying degree of parameters in different models (A–D), we used the Akaike information criterion (AIC) to test model fit. AIC is an estimate of model prediction error taking into account both the goodness of fit and the simplicity of the model. AIC accounts for the amount of information lost while penalizing for the addition of parameters to account for over-fitting. In this study, we used AICc, which adds a modified correction for smaller sample sizes (Hurvich & Tsai, 1989). The smaller the AICc, the better the model fit. Model D yields an AICc of 57.0 (least among all four models) whereas Model A had an AICc of 68.31.

4.3. Forecast Model Sensitivity to Extreme Events

Observational studies have shown that the GS has experienced climate-scale changes in its path variability and instability processes (Andres, 2016; Caesar et al., 2021; Gangopadhyay et al., 2019; Silver et al., 2021), over the past 40 years. These changes include long-term shifts of the path, regime-shift of annual ring formations, and the westward movement of the destabilization point of the GS. Looking ahead, one of the projected impacts of the current rate of global warming is possible future increases in the frequency and amplitude of extreme events (e.g., hurricanes), which are related to atmospheric indices such as the SOI and NAO (Brickman et al., 2018; Wang et al., 2020). The elements of forecast models presented herein (Models A–D) allow us the opportunity to test the sensitivity of the GS forecasts to such extreme atmospheric conditions. We thus repeated the forecast correlation exercise on a number of subsets of previously identified extreme SOI and NAO years during the forecasting period of 1994–2020. Results and interpretations from these sensitivity experiments are presented next.

Model sensitivity to predicting the GSNW for years of different atmospheric extreme events was tested by selecting 1-year predictions from respective years of extreme SOI in one subset of extreme events and of NAO in the other subset. We chose NAO extreme years as it is a more recognized index than either ILL or ILP or its Azores High components. The NAO winter index has a positive correlation of 0.49 with ILL and a negative correlation of 0.78 with ILP. In our models, the impact of buoyancy forcing comes from the ILP/ILL variables and that of the wind-forcing comes from the OCL factor, which is the integrated wind-stress over the basin and over time. The selected set of extreme years (chosen as those falling outside ±0.8 standard deviations) are shown in Figure 6 and are listed in Table 3. The cut off of 0.8 standard deviations was used to allow for a large enough sample size for analysis. All indices were normalized with respect to the mean over the 1980–2019 period before extreme years were selected. This resulted in 12 SOI years, 13 NAO years, and 12 ILL years (Table 3).

For the extreme SOI year subset, 1-year predictions showed the strongest correlation for Model D with $r_f = 0.83$. Models A, B, and C showed values of r_f as 0.50, 0.70, and 0.62, respectively. Model A, the only model without OCL, had the lowest r_f value, which might indicate that OCL is an important predictor for extreme SOI years.

For the extreme NAO year subset, Model C had the highest r_f value with $r_f = 0.62$. Model B had the second highest with $r_f = 0.57$. Model D had similar correlation as Model B ($r_f = 0.54$). Models B and C are the only two models that include OCL, ILP, and ILL indicating that all three variables associated with the NAO

Table 3
Extreme Years (Outside ±0.8 Standard Deviation From the Mean) for Different Atmospheric Indices Used in the Sensitivity Testing

NAO	SOI	ILL
1994	1994	1994
1995	1997	1995
1996	1998	1996
2000	1999	1998
2001	2000	1999
2006	2004	2003
2007	2007	2005
2010	2008	2006
2011	2009	2011
2012	2010	2014
2013	2011	2015
2014	2015	2017
2015	–	–

Note. Also see Figure 6.
Abbreviations: NAO, North Atlantic Oscillation; SOI, Southern Oscillation Index.

might play an important role in predicting extreme NAO years. Interestingly, all of the models outperformed the extreme NAO subsets when compared against the extreme ILL years (third row of Table 4).

The fact that Model D still performed well when predicting the GS path for extreme NAO, SOI, and ILL years (r_f from 0.54 to 0.83) highlights the robustness of the model. However, the model could be further improved for predicting the extreme excursions of the GS by including other important forcings. A challenge for the future is accurately predicting extreme events of different types such as extreme conditions of NAO and SOI, more frequent ring formation, marine heatwaves, more frequent and stronger atmospheric storms. Extreme events may lead to disruption of ecosystems and multiple extreme events may affect the long-term structure of an ecosystem (Gupta et al., 2020). This is an area that is worthy of concentrated research in the future.

In addition to testing the models' ability to predict the GSNW during extreme events, the models' sensitivity to forecasting from an extreme event was also tested. This was done to understand the lasting impact of both buoyancy and wind forcing after an extreme event year. Considering the same extreme event years described above, correlations between the model forecast and TSI were computed for 2 years after an extreme SOI year because the models (A, B, and C) incorporated a 2-year lagged SOI variable. Model A had the lowest correlation ($r_f = 0.22$) with models B, C, and D showing better forecasting performance ($r_f = 0.51, 0.49, 0.47$ respectively). In contrast, for 2 and 3 years after extreme NAO events (some of the models incorporated 2-year lagged ILP and 3-year lagged ILL) there was less difference in forecast correlations between models. Two years after an extreme NAO, Models A, B, C, and D had r_f values of 0.56, 0.55, 0.52, and 0.53, respectively; whereas 3 years after an extreme NAO year, the values of r_f were 0.52, 0.59, 0.53, and 0.72, respectively. Table 4 summarizes the forecast correlation for all these cases. Again, for the 3-year lagged extreme ILL years, all of the models except model A, outperformed the other extreme NAO and SOI subsets (bottom row of Table 4).

Figure 7 shows the τ_x fields for the years with the pressure center being furthest west and furthest east. When the ILL is farthest west, as shown in Figure 7a, the τ_x anomaly over the Labrador region is negative. This negative τ_x anomaly reduces the southward Ekman drift in the region and results in a reduced amount

Table 4
Sensitivity Testing Results for Years Concurrent and Following to the Extreme Events of Different Atmospheric Forcing

Index	Model A	Model B	Model C	Model D
Forecast of extreme event years				
NAO	0.43	0.57	0.62	0.54
SOI	0.50	0.70	0.62	0.83
ILL	0.71	0.84	0.82	0.79
Forecast following extreme event years				
NAO_2	0.56	0.55	0.52	0.53
NAO_3	0.52	0.59	0.53	0.72
SOI_2	0.22	0.51	0.49	0.47
ILL_3	0.48	0.66	0.56	0.65

Note. The top half of the table with row labels NAO, SOI, and ILL, shows the correlation coefficient between model forecasts and the TSI for *concurrent* extreme years listed in Table 3. The bottom half of the table with row labels NAO_2, NAO_3, SOI_2, and ILL_3 shows the correlation coefficients between model forecasts and the TSI for years either 2 or 3 years *following* an extreme event indicated by the subscript number.
Abbreviations: NAO, North Atlantic Oscillation; SOI, Southern Oscillation Index; TSI, Taylor-Stephen Index.

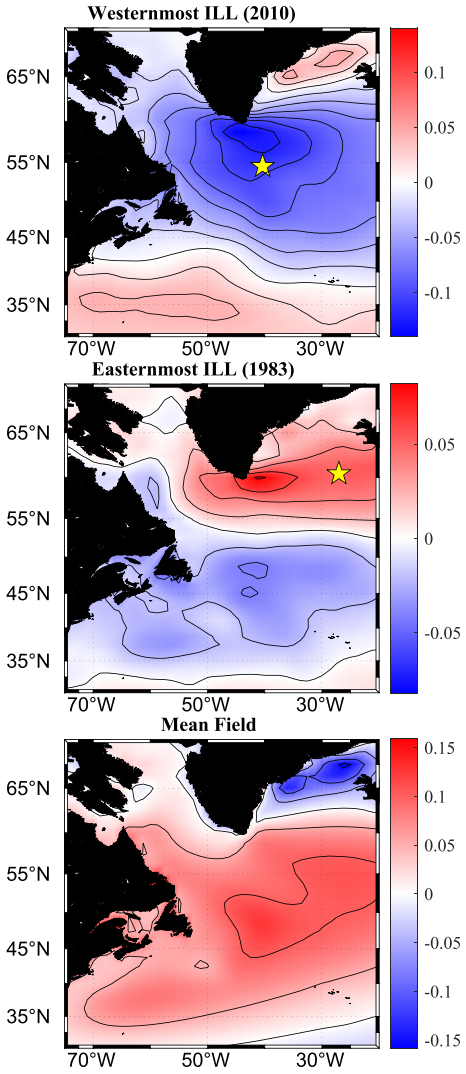

Figure 7. Example of zonal wind stress (τ_x) anomaly for extreme years of ILL with (a) showing the westernmost center for the ILL in 2010, (b) showing easternmost ILL for 1983. (c) shows the mean τ_x field from 1980 to 2019.

of cold Labrador surface water entering the Slope Sea. This allows for a northward shift of the GSNW in later years. SHW16 found that when the ILL was anomalously west, the sea surface temperature over the Labrador Sea and east and south of Greenland was reduced resulting in enhanced deep water convection, decreased amounts of cold water entering the Slope Sea, and a northward shift in the GSNW. In contrast, when the ILL is to the east as shown in Figure 7b, a positive τ_x anomaly appears in this region, increasing the southward advection of Labrador water into the Slope Sea and less deep water convection resulting in a more southward GSNW.

This process is also evident in Figure 8a, which shows the integrated T_E for the 3 years following each extreme ILL event. For years after an extreme westward (eastward) ILL, the integrated T_E is weaker (stronger) resulting in the intersection with T_g occurring at a higher (lower) latitude. This confirms the workings of the Parsons-Veronis hypothesis as presented earlier (Section 3.1) for the years following extreme ILL years as well. This also validates the best performance of Model D, which captures both the effects of buoyancy and wind forcing within a single framework.

The relationship between the SOI and GSNW is less understood and needs further investigation. Figure 8b shows a negative relationship between SOI and OCL for years selected after 2 years of an extreme SOI event. For years with a low (high) SOI, the integrated T_E is weaker (stronger) and the OCL is further north (south). This matches with the Parsons-Veronis idea again as discussed for ILL. However, how exactly the SOI influences the subtropical winds is beyond the scope of this study.

We note in passing that the SOI beta coefficient in all models fitted from 1980 to 2020 was very slightly positive. This is in contradiction to the consistent negative beta coefficients found by SHW16 while analyzing the period from 1966 to 2014. The result presented in Figure 8b was for years mostly before 2014, with 2017 (from the 2015 extreme) being the only years after 2014 (see Table 3) and matches with the negative correlation idea. The changeover of beta coefficients from negative to slightly positive could be in part due to observed changes in the SOI variation in recent years. Power and Smith (2007) found that the mean state of the SOI has decreased in recent years due to climate change. Additionally, Wang et al. (2020) projected that the number of concurrent extreme warm and convective El Nino events will increase under greenhouse warming.

5. Summary and Conclusion

To summarize, we presented a new model (Model D) for forecasting the GS path which includes: (a) the GSNW index from the previous year, (b) gyre-scale integrated Ekman Drift over the past 2 years, and (c) the longitude of Icelandic Low center lagged by 3 years. The forecast correlation over the 27-year period (1994–2020) was 0.65, which is a reasonable improvement from the previous model's (Model A) correlation value of 0.52. This improvement was attributed to the addition of the effect of time-integrated basin-scale wind drift to allow for the BRW to cross the Atlantic to affect the separation of the GS. This also highlights the importance of both North Atlantic pressure cells, Icelandic Low and Azores High in dictating the path of the GS.

The major results from this study can be detailed as follows:

1. The observed separation of the GS path is significantly correlated ($r = 0.55$) with the basin-wide Ekman drift over the subtropical Atlantic integrated over 3 years for over 40 years

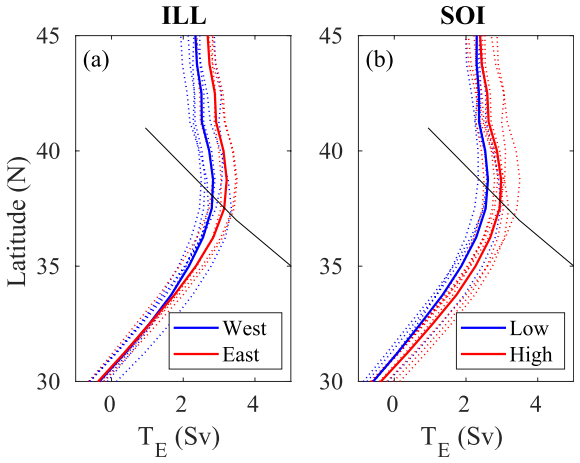

Figure 8. Impact of extreme events on Gulf Stream path forecasting. The meridional distributions of the total Ekman transport (T_E) integrated zonally for 3 years following each occurrence of an extreme ILL to the east (red) or west (blue) are shown in (a). Similar to (a) but for 2 years after an extreme Southern Oscillation Index (SOI) high (red) or low (blue) is shown in (b). Dotted lines show individual years whereas solid lines show the mean. The black line represent the T_g line whose intersection points with T_E represents the outcropping latitude (OCL). Both T_E and T_g are in Sverdrups (The predicted OCL being further north than the observed separation point is due to the loss of fluid not accounted for in the model discussed at the end of Section 3.2).

2. The integrated wind effect was incorporated as an outcropping latitude for the separation point of the GS to improve the forecasting model created earlier in SHW16
3. The model yielding the best results was Model D using the $GSNW_{i-1}$, $OCL2_{i-1}$, and ILL_{i-3} with a forecast correlation of 0.65

SHW16's model was able to predict the TSI with a correlation coefficient of $r_f = 0.52$. We believe that part of this model's success was due to the $GSNW_{i-1}$ variable incorporating the influence of the integrated outcropping latitude into the model (see Table 1). When both $GSNW_{i-1}$ and $OCL2_{i-1}$ are removed the accuracy of the model drops substantially, showing the large role that wind stress is playing on the separation location. The model with the most explained variance for the TSI prediction used only $GSNW_{i-1}$, $OCL2_{i-1}$, and ILL_{i-3}, with a $r_f = 0.65$.

Using both the Azores High and the Icelandic Low parameters in Model D has substantially improved the explained variance to 50% from 36% (with just Icelandic Low as in Model A) for the variability of the GS path between 75 and 65W. Extreme years of SOI or NAO were similarly predictable (Models B and C), which indicates that Model D is able to capture most of the forcing influences from the wind gyres in the North Atlantic and their connection to the equatorial Pacific. However, there is a substantial amount of unexplained variance (40%–45%) which requires future investigation. Some of the factors that may influence the path of the Stream and can be explored in the future are as follows: (a) wind stress curl integrated over basin and time; (b) position of the zero and the maximum of the wind stress curl in the subtropical North Atlantic; (c) strength, intermittency and spatial variability of the DWBC linked with ice melting and convection in the Labrador region; (d) atmospheric forcing strengthening recirculation gyres to the north and south of the Stream. The results presented here open up new research pathways which could utilize long-term data sets now available and advanced numerical models to test similar hypotheses.

Furthermore, the four different models allowed us to carry out a sensitivity study to understand the impacts of extreme events (represented by SOI and NAO indices) on forecasting the GS path. Based on the analysis of a selected subset of years strategically following extreme events during the period 1994–2019, our recommendation is to use Model B (with OCL, SOI and ILP, and ILL indices) in addition to Model D (with OCL and ILL only) and reevaluate the forecast correlations and adapt in the coming 5–10 years.

Finally, the implication of this simple study to understand the climatic variability of the AMOC needs further attention. As presented here, the Parsons-Veronis two-layer idea of Ekman wind drift affecting the GS path is working for four decades in the background of an active AMOC. Given that most of the AMOC variability is in fact dominated by this Ekman Drift (Caesar et al., 2021; Frajka-Williams et al., 2019; Lozier, 2012; Mielke et al., 2013), it is possible that one could use this simpler variability prediction model within the context of a time-varying AMOC predictability scheme when more observations for AMOC would be available.

Data Availability Statement

All data are freely available, and sources are listed in the Data section of the paper. The Taylor-Stephens index (TSI) data can be accessed at http://www.pml-gulfstream.org.uk/. The AZMP data are available from https://www.dfo-mpo.gc.ca/science/data-donnees/azmp-pmza/index-eng.html. The AVISO SSH data are available from https://marine.copernicus.eu/. The JRA-55 wind data are available from https://rda.ucar.edu/datasets/ds628.1/. The SOI data are available from https://climatedataguide.ucar.edu/climate-data/southern-oscillation-indices-signal-noise-and-tahitidarwin-slp-soi (Trenberth, 1984). The atmospheric centers of action indices (for Azores High and Icelandic Low) are available from https://you.stonybrook.edu/coaindices/ (Hameed & Piontkovski, 2004; Hameed & Riemer, 2012). The NAO winter index is available from https://

climatedataguide.ucar.edu/climate-data/hurrell-north-atlantic-oscillation-nao-index-station-based (Hurrell et al., 2003).

Acknowledgments
The authors are grateful for financial supports from NSF (OCE-1851242), SMAST, and UMass Dartmouth. GG was supported by NSF under grants OCE-1657853 and OCE-1558521. The authors gratefully acknowledge the efforts of UCAR, Stoney Brook, and the Japan Meteorological Agency for generating the data that made this paper possible. The authors are thankful to Andre Schmidt for helping with the Matlab and system software while working remotely during COVID-19 for completion of this work and the analysis of multiple years of data. Multiple discussions with Sultan Hameed on Gulf Stream and NAO, and with Chris Wolfe of Stony Brook on winds are appreciated. The authors would like to dedicate this manuscript to the fond memories of many discussions with Professor Geroge Veronis (1926–2019).

References

Anderson, D., & Corry, R. (1985). Ocean response to low frequency wind forcing with application to the seasonal variation in the Florida Straits—Gulf Stream transport. *Progress in Oceanography*, *14*, 7–40. https://doi.org/10.1016/0079-6611(85)90003-5

Andres, M. (2016). On the recent destabilization of the Gulf Stream path downstream of Cape Hatteras. *Geophysical Research Letters*, *43*(18), 9836–9842. https://doi.org/10.1002/2016gl069966

Biastoch, A., Böning, C. W., & Lutjeharms, J. (2008). Agulhas leakage dynamics affects decadal variability in Atlantic Overturning Circulation. *Nature*, *456*(7221), 489–492. https://doi.org/10.1038/nature07426

Brickman, D., Hebert, D., & Wang, Z. (2018). Mechanism for the recent ocean warming events on the Scotian Shelf of eastern Canada. *Continental Shelf Research*, *156*, 11–22. https://doi.org/10.1016/j.csr.2018.01.001

Caesar, L., McCarthy, G., Thornalley, D., Cahill, N., & Rahmstorf, S. (2021). Current Atlantic Meridional Overturning Circulation weakest in last millennium. *Nature Geoscience*, *1–3*, 118–120. https://doi.org/10.1038/s41561-021-00699-z

Caesar, L., Rahmstorf, S., Robinson, A., Feulner, G., & Saba, V. (2018). Observed fingerprint of a weakening Atlantic Ocean overturning circulation. *Nature*, *556*(7700), 191–196. https://doi.org/10.1038/s41586-018-0006-5

Chi, L., Wolfe, C. L., & Hameed, S. (2019). The distinction between the Gulf Stream and its north wall. *Geophysical Research Letters*, *46*(15), 8943–8951. https://doi.org/10.1029/2019gl083775

Cornillon, P. (1986). The effect of the New England Seamounts on Gulf Stream meandering as observed from satellite IR imagery. *Journal of Physical Oceanography*, *16*(2), 386–389. https://doi.org/10.1175/1520-0485(1986)016<0386:teotne>2.0.co;2

Dengg, J. (1996). *The Gulf Stream separation problem. The warmwatersphere of the North Atlantic ocean*. (pp. 254–290).

Drinkwater, K. F. (2004). Atmospheric and sea-ice conditions in the northwest Atlantic during the decade, 1991–2000. *Journal of Northwest Atlantic Fishery Science*, *34*, 1–11. https://doi.org/10.2960/j.v34.m511

Drinkwater, K. F., Belgrano, A., Borja, A., Conversi, A., Edwards, M., Greene, C. H., et al. (2003). The response of marine ecosystems to climate variability associated with the North Atlantic Oscillation. *Geophysical Monograph-American Geophysical Union*, *134*, 211–234. https://doi.org/10.1029/134gm10

Fisheries and Oceans Canada. (2021). *Atlantic zone monitoring program website*. Fisheries and Oceans Canada.

Fofonoff, N. (1954). Steady flow in a frictionless homogeneous ocean. *Journal of Marine Research*, *13*, 254–262.

Frajka-Williams, E., Ansorge, I. J., Baehr, J., Bryden, H. L., Chidichimo, M. P., Cunningham, S. A., et al. (2019). Atlantic meridional overturning circulation: Observed transport and variability. *Frontiers in Marine Science*, *6*, 260. https://doi.org/10.3389/fmars.2019.00260

Gangopadhyay, A., Chaudhuri, A. H., & Taylor, A. H. (2016). On the nature of temporal variability of the Gulf Stream path from 75 to 55 w. *Earth Interactions*, *20*(9), 1–17. https://doi.org/10.1175/ei-d-15-0025.1

Gangopadhyay, A., Cornillon, P., & Watts, D. R. (1992). A test of the Parsons–Veronis hypothesis on the separation of the Gulf Stream. *Journal of Physical Oceanography*, *22*(11), 1286–1301. https://doi.org/10.1175/1520-0485(1992)022<1286:atotph>2.0.co;2

Gangopadhyay, A., Gawarkiewicz, G., Silva, E. N. S., Monim, M., & Clark, J. (2019). An observed regime shift in the formation of warm core rings from the Gulf Stream. *Scientific Reports*, *9*(1), 1–9. https://doi.org/10.1038/s41598-019-48661-9

Gawarkiewicz, G., Chen, K., Forsyth, J., Bahr, F., Mercer, A. M., Ellertson, A., et al. (2019). Characteristics of an advective marine heatwave in the Middle Atlantic Bight in early 2017. *Frontiers in Marine Science*, *6*, 712. https://doi.org/10.3389/fmars.2019.00712

Gawarkiewicz, G., Todd, R. E., Plueddemann, A. J., Andres, M., & Manning, J. P. (2012). Direct interaction between the Gulf Stream and the shelfbreak south of New England. *Scientific Reports*, *2*(1), 1–6. https://doi.org/10.1038/srep00553

Gawarkiewicz, G., Todd, R. E., Zhang, W., Partida, J., Gangopadhyay, A., Monim, M.-U.-H., et al. (2018). The changing nature of shelf-break exchange revealed by the OOI Pioneer Array. *Oceanography*, *31*(1), 60–70. https://doi.org/10.5670/oceanog.2018.110

Gill, A. E. (1982). Atmosphere-ocean dynamics. *International Geophysics Series*, *30*, 662p. https://doi.org/10.1016/s0074-6142(08)x6002-4

Global Monitoring and Forecasting Center. (2021). *Global ocean gridded l4 sea surface heights and derived variables NRT product*. E.U. Copernicus Marine Service Information.

Gupta, A. S., Thomsen, M., Benthuysen, J. A., Hobday, A. J., Oliver, E., Alexander, L. V., et al. (2020). Drivers and impacts of the most extreme marine heatwave events. *Scientific Reports*, *10*(1), 1–15. https://doi.org/10.1038/s41598-020-75445-3

Halliwell, G. R., Jr., & Cornillon, P. (1990). Large-scale SST variability in the western North Atlantic Subtropical Convergence Zone during FASINEX. Part II: Upper ocean heat balance and frontogenesis. *Journal of Physical Oceanography*, *20*(2), 223–234. https://doi.org/10.1175/1520-0485(1990)020<0223:lssvit>2.0.co;2

Hameed, S., & Piontkovski, S. (2004). The dominant influence of the Icelandic Low on the position of the Gulf Stream North Wall. *Geophysical Research Letters*, *31*(9), L09303. https://doi.org/10.1029/2004gl019561

Hameed, S., & Riemer, N. (2012). Relationship of Sahel precipitation and atmospheric centers of action. *Advances in Meteorology*, *2012*, 1–8. https://doi.org/10.1155/2012/953853

Huang, R., & Flierl, G. (1987). Two-layer models for the thermocline and current structure in subtropical/subpolar gyres. *Journal of Physical Oceanography*, *17*(7), 872–884. https://doi.org/10.1175/1520-0485(1987)017<0872:tlmftt>2.0.co;2

Huesmann, A. S., & Hitchman, M. H. (2003). The 1978 shift in the NCEP reanalysis stratospheric quasi-biennial oscillation. *Geophysical Research Letters*, *30*(2), 1048. https://doi.org/10.1029/2002gl016323

Hurrell, J. W., Brown, S. J., Trenberth, K. E., & Christy, J. R. (2000). Comparison of tropospheric temperatures from radiosondes and satellites: 1979–98. *Bulletin of the American Meteorological Society*, *81*(9), 2165–2177. https://doi.org/10.1175/1520-0477(2000)081<2165:cottfr>2.3.co;2

Hurrell, J. W., Kushnir, Y., Ottersen, G., & Visbeck, M. (2003). An overview of the North Atlantic Oscillation. *Geophysical Monograph-American Geophysical Union*, *134*, 1–35. https://doi.org/10.1029/134gm01

Hurrell, J. W., Kushnir, Y., & Visbeck, M. (2001). The North Atlantic Oscillation. *Science*, *291*(5504), 603–605. https://doi.org/10.1126/science.1058761

Hurvich, C. M., & Tsai, C.-L. (1989). Regression and time series model selection in small samples. *Biometrika*, *76*(2), 297–307. https://doi.org/10.1093/biomet/76.2.297

Inkscape Project. (2020). *Inkscape 1.0.1*. Retrieved from https://inkscape.org

Japan Meteorological Agency. (2013). *JRA-55: Japanese 55-year reanalysis, monthly means and variances*. Research data archive at the National Center for Atmospheric Research. https://doi.org/10.5065/D60G3H5B
Joyce, T. M., Kwon, Y.-O., & Yu, L. (2009). On the relationship between synoptic wintertime atmospheric variability and path shifts in the Gulf Stream and the Kuroshio extension. *Journal of Climate*, *22*(12), 3177–3192. https://doi.org/10.1175/2008jcli2690.1
Kistler, R., Kalnay, E., Collins, W., Saha, S., White, G., Woollen, J., et al. (2001). The NCEP–NCAR 50-year reanalysis: Monthly means CD-ROM and documentation. *Bulletin of the American Meteorological Society*, *82*(2), 247–267. https://doi.org/10.1175/1520-0477(2001)082<0247:tnnyrm>2.3.co;2
Lee, T., & Cornillon, P. (1996). Propagation and growth of Gulf Stream meanders between 75 and 45 w. *Journal of Physical Oceanography*, *26*(2), 225–241. https://doi.org/10.1175/1520-0485(1996)026<0225:pagogs>2.0.co;2
Lozier, M. S. (2010). Deconstructing the conveyor belt. *Science*, *328*(5985), 1507–1511. https://doi.org/10.1126/science.1189250
Lozier, M. S. (2012). Overturning in the North Atlantic. *Annual Review of Marine Science*, *4*, 291–315. https://doi.org/10.1146/annurev-marine-120710-100740
Lozier, M. S., Bacon, S., Bower, A. S., Cunningham, S. A., De Jong, M. F., De Steur, L., et al. (2017). Overturning in the subpolar North Atlantic program: A new international ocean observing system. *Bulletin of the American Meteorological Society*, *98*(4), 737–752. https://doi.org/10.1175/bams-d-16-0057.1
McCarthy, G. D., Joyce, T. M., & Josey, S. A. (2018). Gulf Stream variability in the context of quasi-decadal and multidecadal Atlantic climate variability. *Geophysical Research Letters*, *45*(20), 11–257. https://doi.org/10.1029/2018gl079336
Mielke, C., Frajka-Williams, E., & Baehr, J. (2013). Observed and simulated variability of the AMOC at 26 n and 41 n. *Geophysical Research Letters*, *40*(6), 1159–1164. https://doi.org/10.1002/grl.50233
Mills, K. E., Pershing, A. J., Brown, C. J., Chen, Y., Chiang, F.-S., Holland, D. S., et al. (2013). Fisheries management in a changing climate: Lessons from the 2012 ocean heat wave in the northwest Atlantic. *Oceanography*, *26*(2), 191–195. https://doi.org/10.5670/oceanog.2013.27
Nye, J. A., Joyce, T. M., Kwon, Y.-O., & Link, J. S. (2011). Silver hake tracks changes in northwest Atlantic circulation. *Nature Communications*, *2*(1), 1–6. https://doi.org/10.1038/ncomms1420
Parsons, A. (1969). A two-layer model of Gulf Stream separation. *Journal of Fluid Mechanics*, *39*(3), 511–528. https://doi.org/10.1017/s0022112069002308
Pershing, A. J., Alexander, M. A., Hernandez, C. M., Kerr, L. A., Le Bris, A., Mills, K. E., et al. (2015). Slow adaptation in the face of rapid warming leads to collapse of the Gulf of Maine cod fishery. *Science*, *350*(6262), 809–812. https://doi.org/10.1126/science.aac9819
Power, S. B., & Smith, I. N. (2007). Weakening of the walker circulation and apparent dominance of El Niño both reach record levels, but has ENSO really changed? *Geophysical Research Letters*, *34*(18), L18702. https://doi.org/10.1029/2007gl030854
Quenouille, M. (1951). The variate-difference method in theory and practice. *Revue de l'Institut International de Statistique*, *19*, 121–129. https://doi.org/10.2307/1401239
Rossby, T. (1999). On gyre interactions. *Deep Sea Research Part II: Topical Studies in Oceanography*, *46*(1–2), 139–164. https://doi.org/10.1016/s0967-0645(98)00095-2
Rossby, T., & Benway, R. (2000). Slow variations in mean path of the Gulf Stream east of Cape Hatteras. *Geophysical Research Letters*, *27*(1), 117–120. https://doi.org/10.1029/1999gl002356
Sanchez-Franks, A., Hameed, S., & Wilson, R. E. (2016). The Icelandic Low as a predictor of the Gulf Stream north wall position. *Journal of Physical Oceanography*, *46*(3), 817–826. https://doi.org/10.1175/jpo-d-14-0244.1
Schoonover, J., Dewar, W. K., Wienders, N., & Deremble, B. (2017). Local sensitivities of the Gulf Stream separation. *Journal of Physical Oceanography*, *47*(2), 353–373. https://doi.org/10.1175/jpo-d-16-0195.1
Silver, A., Gangopadhyay, A., Gawarkiewicz, G., Silva, E. N. S., & Clark, J. (2021). Interannual and seasonal asymmetries in Gulf Stream ring formations from 1980 to 2019. *Scientific Reports*, *11*(1), 1–7. https://doi.org/10.1038/s41598-021-81827-y
Smeed, D., McCarthy, G., Rayner, D., Moat, B., Johns, W., Baringer, M., & Meinen, C. (2016). *Atlantic Meridional Overturning Circulation observed by the RAPID-MOCHA-WBTS (rapid-meridional overturning circulation and heatflux array-western boundary time series) array at 26n from 2004 to 2015*. British Oceanographic Data Centre/Natural Environment Research Council.
Spall, M. A. (1996). Dynamics of the Gulf Stream/deep western boundary current crossover. Part II: Low-frequency internal oscillations. *Journal of Physical Oceanography*, *26*(10), 2169–2182. https://doi.org/10.1175/1520-0485(1996)026<2169:dotgsw>2.0.co;2
Sturaro, G. (2003). A closer look at the climatological discontinuities present in the NCEP/NCAR reanalysis temperature due to the introduction of satellite data. *Climate Dynamics*, *21*(3–4), 309–316. https://doi.org/10.1007/s00382-003-0334-4
Taylor, A. H. (1995). North–south shifts of the Gulf Stream and their climatic connection with the abundance of zooplankton in the UK and its surrounding seas. *ICES Journal of Marine Science*, *52*(3–4), 711–721. https://doi.org/10.1016/1054-3139(95)80084-0
Taylor, A. H., & Gangopadhyay, A. (2001). A simple model of interannual displacements of the Gulf Stream. *Journal of Geophysical Research*, *106*(C7), 13849–13860. https://doi.org/10.1029/1999jc000147
Taylor, A. H., Jordan, M. B., & Stephens, J. A. (1998). Gulf Stream shifts following ENSO events. *Nature*, *393*(6686), 638. https://doi.org/10.1038/31380
The MathWorks, I. (2020). *Mapping toolbox [Computer software manual]*. Retrieved from https://www.mathworks.com/help/map/index.html
Thompson, J. D., & Jr, W. S. (1989). A limited-area model of the Gulf Stream: Design, initial experiments, and model-data intercomparison. *Journal of Physical Oceanography*, *19*(6), 791–814. https://doi.org/10.1175/1520-0485(1989)019<0791:alamot>2.0.co;2
Tracey, K. L., & Watts, D. R. (1986). On Gulf Stream meander characteristics near Cape Hatteras. *Journal of Geophysical Research*, *91*(C6), 7587–7602. https://doi.org/10.1029/jc091ic06p07587
Trenberth, K. E. (1984). Signal versus noise in the Southern Oscillation. *Monthly Weather Review*, *112*(2), 326–332. https://doi.org/10.1175/1520-0493(1984)112<0326:svnits>2.0.co;2
Veronis, G. (1973). Model of world ocean circulation. 1. Wind-driven, 2-layer. *Journal of Marine Research*, *31*(3), 228–288.
Walker, G., & Bliss, E. (1932). Memoirs of the royal meteorological society. *Quarterly Journal of the Royal Meteorological Society*, *4*(36), 53.
Wang, G., Cai, W., & Santoso, A. (2020). Stronger increase in the frequency of extreme convective than extreme warm El Niño events under greenhouse warming. *Journal of Climate*, *33*(2), 675–690. https://doi.org/10.1175/jcli-d-19-0376.1
Weisberg, S. (2005). *Applied linear regression* (Vol. 528). John Wiley & Sons.
Zhang, R., Sutton, R., Danabasoglu, G., Kwon, Y.-O., Marsh, R., Yeager, S. G., et al. (2019). A review of the role of the Atlantic Meridional Overturning Circulation in Atlantic multidecadal variability and associated climate impacts. *Reviews of Geophysics*, *57*(2), 316–375. https://doi.org/10.1029/2019rg000644

Zhang, R., & Vallis, G. K. (2007). The role of bottom vortex stretching on the path of the North Atlantic western boundary current and on the northern recirculation gyre. *Journal of Physical Oceanography*, *37*(8), 2053–2080. https://doi.org/10.1175/jpo3102.1

Zhao, J., & Johns, W. (2014a). Wind-driven seasonal cycle of the Atlantic Meridional Overturning Circulation. *Journal of Physical Oceanography*, *44*(6), 1541–1562. https://doi.org/10.1175/jpo-d-13-0144.1

Zhao, J., & Johns, W. (2014b). Wind-forced interannual variability of the Atlantic Meridional Overturning Circulation at 26.5 n. *Journal of Geophysical Research: Oceans*, *119*(4), 2403–2419. https://doi.org/10.1002/2013jc009407